Dynamic nonlinear screening of slow ions in an electron gas

A. Salin
Laboratoire de Physico-Chimie Moléculaire, UMR 5803 CNRS-Université Bordeaux I, 351 Cours de la Libération, 33405 Talence, France and Departamento de Física de Materiales, Universidad del País Vasco/Euskal Herriko Unibertsitatea, Apartado 1072, 20080 Donostia/San Sebastián, Spain

A. Arnau and P. M. Echenique
Departamento de Física de Materiales, Universidad del País Vasco/Euskal Herriko Unibertsitatea, Apartado 1072, 20080 Donostia/San Sebastián, Spain

E. Zaremba
Department of Physics, Queen's University, Kingston, Ontario, Canada K7L 3N6
(Received 22 June 1998)

We have used the ensemble Kohn-Sham method with the local-density approximation to determine self-consistently the dynamic screening cloud around an impurity moving adiabatically through a uniform electron gas with velocity below the Fermi velocity. The asymmetry of the induced field and electronic density caused by the impurity motion is fully taken into account. We discuss the forward-backward asymmetry for the case of bare positive and negative charges as well as for hydrogen atoms. We show that the stopping power of the electron gas varies linearly with the projectile velocity up to velocities close to the Fermi velocity. We study the asymmetry of the bound states, its contribution to the stopping power and the evolution of the binding energy as a function of projectile velocity. Finally, we give a complete derivation of the low energy behavior of the stopping power and the generalization of the Friedel sum rule and oscillations for the case of moving impurities. [S0163-1829(99)03104-5]

I. INTRODUCTION

The dynamic screening of charges moving through an electron gas is a complex theoretical problem that has been used for years to model the interaction of ions with condensed matter at various degrees of approximation. Since the early works of Fermi and Teller,[1] Bohm and Pines,[2] Lindhard,[3] Neufeld and Ritchie[4] in the 50's, most studies have been restricted to the linear response regime within the random-phase approximation.[5] At this level of approximation the response of the electronic system to an external perturbation is treated self-consistently and includes both plasmon (collective) and electron-hole pair (single particle) excitations. However, results obtained within this framework are only quantitatively accurate as long as $Z/v \ll 1$, where Z is the ion charge and v the relative velocity of the collision between the moving ion and the target electrons (it is essentially the ion velocity for fast ions and the mean electron velocity for slow ions). In practice, this restricts the applicability of linear theory to small charges, fast ions or materials with large electron densities.

There have been various attempts to go beyond linear response theory: (i) quadratic response function approaches,[6] which give the next-higher-order correction in a perturbative expansion in powers of the ion charge Z, (ii) semiclassical hydrodynamic descriptions of the electron gas treated as a fluid that responds to the external field created by the moving ion,[7,8] and (iii) a scattering approach within the nonlinear screening model based on density functional theory as applied to a static impurity in an electron gas.[9] The latter approach is restricted to slow ions.[10]

Recently, Zaremba, Arnau, and Echenique[11] extended the nonlinear screening theory to finite velocities by making use of the shifted Fermi sphere description introduced by Schönhammer.[12] However, rather than treating the interaction between the electrons and projectile rigorously, a spherical average approximation to the interaction potential was used. In the present work we avoid this approximation and perform a fully nonlinear self-consistent calculation of the screening of a moving charge by an electron gas in the adiabatic limit (steady-state situation) using density-functional theory. We focus our study on quantities that characterize the screening, like the self-consistent screened potential and charge densities, and the force exerted by the medium on the moving ion that defines the stopping power.

Atomic units are used unless otherwise stated.

II. THEORY

We consider the problem of a charge Z moving with a constant velocity v through an electron gas which, in the absence of the ion, is homogeneous. In the projectile frame, the electrons stream past the ion and scatter from the effective potential established by the mutual Coulomb interactions between the ion and electrons, and between the electrons themselves. This dynamic state is achieved by means of an adiabatic evolution of the electron gas from its initial homogeneous distribution to the final state in which the ion is dynamically screened.[12] In this picture, the electronic states are characterized by their asymptotic momentum $\boldsymbol{k}$ and, in

the projectile frame, the set of occupied states belongs to a Fermi sphere in $\boldsymbol{k}$ space the origin of which is at $\boldsymbol{k}=-\boldsymbol{v}$. We name this adiabatic approach the shifted Fermi sphere approximation. One of our objectives is to determine self-consistently the effective scattering potential; by the nature of the problem, this potential has cylindrical symmetry.

To solve this problem we make use of the Kohn-Sham formulation of density-functional theory within the local-density approximation.[13] We have therefore to solve a one-electron Schrödinger equation having the form

$$[-\tfrac{1}{2}\nabla^2+V(\boldsymbol{r})-\epsilon]\psi_\epsilon(\boldsymbol{r})=0, \tag{1}$$

where the potential $V(\boldsymbol{r})$ is the sum of the projectile potential, Hartree potential $V_{\rm H}(\boldsymbol{r})$ and exchange-correlation potential $V_{\rm xc}(\boldsymbol{r})$. The electronic orbitals are here labeled by the energy variable ϵ, which can correspond to either continuum scattering states or bound states if the latter exist. In either case, their angular dependence can be expanded in terms of spherical harmonics:

$$\psi_\epsilon(\boldsymbol{r})=\sum_{lm} u_{lm}(r;\epsilon)Y_{lm}(\hat{\boldsymbol{r}})/r. \tag{2}$$

The notation $\hat{\boldsymbol{r}}$ designates a unit vector along the direction of $\boldsymbol{r}$. The cylindrical symmetry of the potential allows an expansion of the form

$$V(\boldsymbol{r})=\sum_{\nu} V_\nu(r)P_\nu(\cos\theta), \tag{3}$$

where P_ν is a Legendre polynomial. An important consequence of the nonspherical symmetry of the potential is that the radial functions $u_{lm}(r;\epsilon)$ satisfy a system of coupled equations

$$\left[\frac{d^2}{dr^2}+2\epsilon-\frac{l(l+1)}{r^2}\right]u_{lm}(r;\epsilon)=2\sum_{l'} U^m_{ll'}u_{l'm}(r;\epsilon), \tag{4}$$

where

$$U^m_{ll'}(r)=\int d\hat{\boldsymbol{r}}\, Y^*_{lm}(\hat{\boldsymbol{r}})V(r,\theta)Y_{l'm}(\hat{\boldsymbol{r}}). \tag{5}$$

It can be shown that the components $V_\nu(r)$ of the potential satisfy the conditions

$$\lim_{r\to 0}V_\nu(r)\sim\begin{cases} r^\nu & \text{if} \quad \nu\neq 0, \\ -\dfrac{Z}{r} & \text{if} \quad \nu=0. \end{cases} \tag{6}$$

The system of coupled equations is solved numerically after truncation of the partial wave expansion to a maximum value $l_{\rm max}$. In practice, we have used values of $l_{\rm max}$ up to 15. The number of terms in Eq. (3) has been limited to $\nu_{\rm max}$. Most calculations have been done with $\nu_{\rm max}=2$ (i.e., inclusion of monopole, dipole, and quadrupole components) but some tests have been performed with $\nu_{\rm max}=3$.

A. Determination of the density

1. Continuum orbitals

The continuum solutions of Eq. (1), normalized on the $\boldsymbol{k}$ scale, are labeled as $\psi_{\boldsymbol{k}}(\boldsymbol{r})$ and satisfy the asymptotic condition

$$\psi_{\boldsymbol{k}}(\boldsymbol{r})\to_{r\to\infty}(2\pi)^{-3/2}\left[e^{i\boldsymbol{k}\cdot\boldsymbol{r}}+f(\boldsymbol{k},\hat{\boldsymbol{r}})\frac{e^{ikr}}{r}\right]. \tag{7}$$

As the potential is not spherically symmetric, the radial functions $u_{lm}(r;\boldsymbol{k})$ will depend on the direction $\hat{\boldsymbol{k}}$ of the incident plane wave. For a given m, we determine $(l_{\rm max}+1)$ linearly independent solutions of the system (4), i.e. $(l_{\rm max}+1)$ sets $\{u^{(j)}_l, l=0,l_{\rm max}\}$ where j varies from 0 to $l_{\rm max}$. The required solution may always be expressed as a linear combination of these linearly independent solutions

$$u_{lm}(r;\boldsymbol{k})=\sum_j \gamma^m_j(\boldsymbol{k})u^{(j)}_{lm}(r;k), \tag{8}$$

where each solution varies asymptotically as

$$u^{(j)}_{lm}(r;k)\to_{r\to\infty}[A^m_{lj}(k)\sin(kr-l\pi/2) + B^m_{lj}(k)\cos(kr-l\pi/2)]. \tag{9}$$

From the asymptotic condition (7), one finds

$$\psi_{\boldsymbol{k}}(\boldsymbol{r})=(2\pi)^{-3/2}\frac{4\pi}{kr}\sum_{jll'm} i^{l'}\Gamma^m_{jl'}(k)Y^*_{l'm}(\hat{\boldsymbol{k}}) \times Y_{lm}(\hat{\boldsymbol{r}})u^{(j)}_{lm}(r;k), \tag{10}$$

where the matrix $\boldsymbol{\Gamma}^m(k)$ is

$$\boldsymbol{\Gamma}^m(k)=[\boldsymbol{A}^m(k)-i\boldsymbol{B}^m(k)]^{-1} \tag{11}$$

and the elements of the $\boldsymbol{A}$ and $\boldsymbol{B}$ matrices are defined in Eq. (9). For completeness, we quote the expression for the scattering amplitude of an electron scattering into the final direction $\hat{\boldsymbol{k}}'$:

$$f(\boldsymbol{k},\hat{\boldsymbol{k}}')=\frac{2\pi}{ik}\sum_{ll'm} Y_{lm}(\hat{\boldsymbol{k}}')Y^*_{l'm}(\hat{\boldsymbol{k}})\{i^{l'-l}S^m_{ll'}(k)-\delta_{ll'}\}, \tag{12}$$

where

$$\boldsymbol{S}^m(k)=[\boldsymbol{A}^m(k)+i\boldsymbol{B}^m(k)]\boldsymbol{\Gamma}^m(k),$$

is the S matrix of the nonspherical scattering potential.

There is a simple way to generate a set of independent solutions of the system of coupled equations (4). Using the form of the coupling terms for small r it can be shown that there exist solutions behaving as

$$u^{(j)}_{lm}(r;k)\sim_{r\to 0} r^{j+|l-j|+1}\sum_{i=1}^{\infty} b^l_i r^{i-1}, \tag{13}$$

which provides the required set of independent solutions in the vicinity of the origin. We use the Taylor series expansion (13) to solve the system of coupled equations (4) close to the origin and then switch to the Numerov method for larger values of r.

Once we have determined the wave functions $\psi_{\boldsymbol{k}}$, we need to calculate the density $n_C(\boldsymbol{r})$. Using an expansion of the density in Legendre polynomials

$$n_C(\boldsymbol{r})=\sum_L n_L^C(r)P_L(\cos\theta_r), \tag{14}$$

we obtain the expression

$$n_L^C(r)=\frac{1}{(2\pi r)^2}\sum_{ll'm}\sum_{jj'}\begin{Bmatrix} l & l' & L \\ m & -m & 0\end{Bmatrix} \times\int dk\ \Xi^m_{jj'}(k)u^{(j)}_{lm}(r;k)u^{(j')}_{l'm}(r;k) \tag{15}$$

$$\Xi^m_{jj'}(k)=\sum_{\lambda\lambda'} i^{\lambda-\lambda'}\Gamma^m_{j\lambda}(k)[\Gamma^m_{j'\lambda'}(k)]^*\mathcal{C}^m_{\lambda\lambda'}(k) \tag{16}$$

$$\mathcal{C}^m_{\lambda\lambda'}(k)=\sum_{L'}\begin{Bmatrix} \lambda & \lambda' & L' \\ -m & m & 0\end{Bmatrix}C_{L'}(k). \tag{17}$$

The angular coefficients are defined in terms of Wigner $3j$ symbols

$$\begin{Bmatrix} l & l' & L \\ m & -m & 0\end{Bmatrix}=(-)^m(2L+1)(2l+1)^{1/2}(2l'+1)^{1/2} \times\begin{pmatrix} l & l' & L \\ 0 & 0 & 0\end{pmatrix}\begin{pmatrix} l & l' & L \\ m & -m & 0\end{pmatrix}. \tag{18}$$

The auxiliary function $C_L(k)$ comes from the angular integration over $\boldsymbol{k}$ for a shifted Fermi sphere

$$\begin{aligned} C_L(k)&=(-)^L\int_{y_m(k)}^1 dy\ P_L(y)\\ &=(-)^L[1-y_m(k)]\quad L=0\\ &=(-)^L(1-y_m^2)^{1/2}P_L^1(y_m)/L(L+1)\quad L\geqslant 1,\end{aligned} \tag{19}$$

where $y_m=(k^2+v^2-k_F^2)/2kv$ for $|k_F-v|<k<k_f+v$ and, when $k_F>v$, $y_m=-1$ for $0<k<k_F-v$. The function $C_L(k)$ is zero when the latter conditions on k are not met.

In practice we calculate the density change Δn^C by substracting from n_C the expression obtained for the homogenous system in the absence of the ion in which case the Kohn-Sham orbitals are plane waves, i.e., $\phi_{\boldsymbol{k}}(\boldsymbol{r})=(2\pi)^{-3/2}\exp(i\boldsymbol{k}\cdot\boldsymbol{r})$.

2. Bound orbitals

The bound orbitals are determined in the usual way by performing an outward integration of the Kohn-Sham equation from $r=0$ followed by an inward integration from infinity, and then matching both solutions at some intermediate distance. The only difference with respect to the case of a spherical potential is that now we get a set of $l_{\max}+1$ linearly independent solutions $u^{(j)}_{lm}$ when starting from the origin and $l_{\max}+1$ linearly independent solutions $v^{(j)}_{lm}$ when starting the integration from infinity. The set of linearly independent solutions for the outward integration is determined in the same way as for the continuum states. For the inward integration we use the asymptotic condition

$$v^{(j)}_{lm}\sim_{r\to\infty}\delta_{jl}\ \exp[-r\sqrt{-2\epsilon}]. \tag{20}$$

If a bound state exists, then there is a linear combination of the functions $u^{(j)}_{lm}$ that can be identified with a linear combination of the functions $v^{(j)}_{lm}$, namely,

$$\sum_j \mu_j u^{(j)}_{lm}(r;\epsilon)=\sum_i \lambda_i v^{(i)}_{lm}(r;\epsilon)$$

$$\sum_j \mu_j \frac{d}{dr}u^{(j)}_{lm}(r;\epsilon)=\sum_i \lambda_i \frac{d}{dr}v^{(i)}_{lm}(r;\epsilon). \tag{21}$$

This set of $2l_{\max}+2$ homogeneous equations has a nontrivial solution if and only if the determinant is zero, which generalizes the Wronskian condition for the case of spherical potentials. The search for bound-state energies is thus made equivalent to a search for the zeroes of the determinant of the system (21). However, in practice, we avoid using the derivative of the functions by constructing an equivalent condition in terms of the values of the functions at two different distances. Once the bound-state energy has been determined, the corresponding eigenfunction $\psi_\epsilon(\boldsymbol{r})$ is determined by a singular value decomposition[14] of the system (21).

The density produced by the bound states $n_B(\boldsymbol{r})$ can now be calculated from

$$n_L^B(r)=\frac{1}{4\pi r^2}\sum_{ll'm}\begin{Bmatrix} l & l' & L \\ m & -m & 0\end{Bmatrix}u^m_l(r;\epsilon)u^m_{l'}(r;\epsilon), \tag{22}$$

where $u^m_l(r;\epsilon)$ is the l component of $\psi_\epsilon(\boldsymbol{r})$ as defined in Eq. (2). Once the total density change $\Delta n(\boldsymbol{r})=n^B(\boldsymbol{r})+\Delta n^C(\boldsymbol{r})$ is known, the Hartree and exchange-correlation potentials are calculated and the resulting total potential is then used in the next step of the iteration cycle. This process is continued until convergence is obtained.

In the projectile frame, the bound density (summing to a total of N_B electrons) is fixed on the ion, and so in the gas frame it is carried along with the projectile. The continuum density corresponds to a flux of electrons colliding with the projectile, having on average the velocity $-\boldsymbol{v}$ in the projectile frame. The scattering of these continuum electrons from the projectile gives rise to an accumulation (or depletion) of charge that, in our adiabatic approximation, is stationary in the projectile frame. This charge accumulation (or depletion) moves with the projectile in the gas frame. It sums to a total charge $Z-N_B$ that also moves with the projectile. So, the generalized Friedel sum rule derived in Appendix B determines the number of electrons (Z) associated with the net total electronic flux caused by the projectile motion.

Two further remarks are in order concerning the shifted-Fermi sphere approximation. First, *in our adiabatic approximation* and in the projectile frame, we have to solve a *stationary* problem in which the screening charge is not that of the ground-state density of the system projectile+jellium [which would correspond to the use of a Fermi distribution of continuum orbitals, i.e., the integration over k in Eq. (15) would be from zero to k_F with $C_L(k)=2$]. In fact, the screening charge corresponds to an ensemble density deter-

mined by the function $C_L(k)$, defined in Eq. (19). It satisfies the condition for the validity of the Hohenberg-Kohn theorem for ensembles when $v<k_F$ (see Ref. 13, Sec. 3.5): $C_L(k)$ never increases with increasing k. Under the same condition, a Kohn-Sham scheme can also be devised that validates the approach described above to solve the problem *in the adiabatic approximation*. Of course, the exchange-correlation energy functional is not the same for the ensemble as for the ground state of the system. In spite of that, we make use of the local-density approximation (LDA) based on the energy functional for the ground state of a homogeneous electron gas. We may note that a homogenous system is translationally invariant (in other words, the exchange-correlation energy is the same for a shifted and unshifted Fermi distribution). Still, further examination of the validity of this particular form of local approximation for our case is clearly required.

Second, as concerns the bound states, we have, in some cases, set the occupation of certain bound orbitals to zero. Such a procedure has been used previously to study multicharged ions embedded in a metal[15] but it cannot be justified within the ensemble Kohn-Sham scheme. Nevertheless, it is of interest to carry out such calculations to investigate the nature of the screening in various situations. For example, in the case of a proton projectile, we allow for the population of the bound state to be zero, one or two electrons which, respectively, corresponds to proton, neutral hydrogen (H), and negative ion (H^-) projectiles. We will use this terminology hereafter. Of course the energy loss we calculate will correspond to a *single* charge state. Any comparison of our results with experiment would require some average over various charge states.[16]

B. Determination of the Hartree potential

The Hartree potential is determined from a solution of Poisson's equation. However, in order to numerically stabilize the iterative procedure, we in fact introduce a damped Poisson equation in which the potential for the nth iteration involves the one from the (n-1)th iteration:

$$\left[\frac{1}{r}\frac{d^2}{dr^2}r-\frac{\nu(\nu+1)}{r^2}-\kappa^2\right]V_\nu^{H,n}(r) = -4\pi\Delta n_\nu^{n-1}(r)-\kappa^2 V_\nu^{H,n-1}(r)=-4\pi F_\nu^{n-1}. \tag{23}$$

The introduction of the parameter κ (typically of the order of one atomic unit) effectively eliminates the long-range nature of the Coulomb potential, which is the source of the numerical instability. However, at convergence the artificial κ-dependent terms cancel and one recovers the true form of the Hartree potential. The solution of Eq. (23) is given by

$$V_\nu^{H,n}(r)=4\pi\kappa\left\{\tilde{h}_\nu^{(1)}(\kappa r)\int_0^r dr'\, r'^2\tilde{j}_\nu(\kappa r')F_\nu^{n-1}(r') + \tilde{j}_\nu(\kappa r)\int_r^\infty dr'\, r'^2\tilde{h}_\nu^{(1)}(\kappa r')F_\nu^{n-1}(r')\right\}, \tag{24}$$

where the functions $\tilde{j}_\nu$ and $\tilde{h}_\nu^{(1)}$ are modified spherical Bessel functions defined in terms of modified Bessel functions of fractional order by

$$\tilde{j}_\nu(x)=\sqrt{\frac{\pi}{2x}}I_{\nu+(1/2)}(x) \tag{25}$$

$$\tilde{h}_\nu^{(1)}(x)=(-)^{\nu+1}\sqrt{\frac{2}{\pi x}}K_{\nu+(1/2)}(x). \tag{26}$$

The functions I and K are defined as in Ref. 17. The integrals in Eq. (24) are calculated in a cumulative fashion using Simpson's rule to generate the potential at every second point on the radial mesh; this is then followed by an interpolation to yield the potential on the full radial mesh.

C. Exchange-correlation potential

Our exchange-correlation potential is based on the exchange-correlation potential $\mu_{\rm xc}[n]$ for a static homogenous system of density n. Therefore, it does not include any dynamic contribution. In practice we use the expression given in Ref. 18. The potential $V_{\rm xc}$ is in fact the change in exchange-correlation potential caused by the presence of the external charge: $V_{\rm xc}=\mu_{\rm xc}[\Delta n(\boldsymbol{r})+n_0]-\mu_{\rm xc}[n_0]$. The component of $V_{\rm xc}$ for a given value of ν is given by

$$V_\nu^{\rm xc}(r)=(\nu+\tfrac{1}{2})\int_{-1}^{+1}d(\cos\theta)V_{\rm xc}(\boldsymbol{r})P_\nu(\cos\theta). \tag{27}$$

In our calculations, we keep a finite number of terms in the expansion of the potential over Legendre polynomials and call $\nu_{\max}$ the corresponding maximum value of ν in (3). Assuming that $\nu\leqslant\nu_{\max}$, $V_{\rm xc}(\boldsymbol{r})$ is a polynomial in $\cos\theta$ of order $\nu_{\max}$ at most, in which case the integrand is a polynomial of order $2\nu_{\max}$ at most, for which the integral is given exactly by a Gaussian quadrature of order $\nu_{\max}+1$. If x_i and ω_i are the pivots and weights of such a quadrature ($i=1,\nu_{\max}+1$),

$$V_\nu^{\rm xc}(r)=\sum_{i=1}^{\nu_{\max}+1}\Omega_{i,\nu}V_{\rm xc}(r,\cos^{-1}x_i), \tag{28}$$

$$\Omega_{i,\nu}=(\nu+\tfrac{1}{2})\omega_i P_\nu(x_i). \tag{29}$$

D. Calculation of stopping power

A charge Z traveling with velocity $\boldsymbol{v}$ through the electronic density $n(\boldsymbol{r})$ experiences a force along $\boldsymbol{v}$ equal to

$$F=\lim_{R\to 0}\hat{\boldsymbol{v}}\cdot\boldsymbol{\nabla}_{\boldsymbol{R}}\int d\boldsymbol{r}\, n(\boldsymbol{r})\frac{Z}{|\boldsymbol{r}-\boldsymbol{R}|}, \tag{30}$$

where $\boldsymbol{R}(t)$ is the projectile position. As a uniform density produces no force, we can replace n by Δn. Using the expansion of $V_{\rm H}$ in Legendre polynomials and the limit (6) for small distances, the energy loss per unit path length is

$$\frac{dE}{dR}=Z\lim_{R\to 0}V_1^{\rm H}(R)/R. \tag{31}$$

The energy loss is directly related to the dipole part of the Hartree potential. It is interesting to note that the above result provides a simple connection between the dipole part of the Hartree potential near the origin and the transport cross section since the energy loss may be determined from the latter in the usual way.[19] The average energy transferred by an electron with momentum $\boldsymbol{k}$ to an infinitely massive particle having velocity $\boldsymbol{v}$ is given by v times the average of the electron momentum change along $\hat{\boldsymbol{v}}$. Then the energy loss per unit path length is (summing over a shifted Fermi sphere in $\boldsymbol{k}$ space)

$$\frac{dE}{dR}=\frac{1}{4\pi^3}\int^{\mathrm{SFS}} d\boldsymbol{k}\, k^2\sigma_{\boldsymbol{v}}^{\mathrm{tr}}, \tag{32}$$

where $\sigma_{\boldsymbol{v}}^{\mathrm{tr}}$ is the component along $\boldsymbol{v}$ of the transport cross section (a vector quantity when the potential is not spherically symmetric)

$$\sigma_{\boldsymbol{v}}^{\mathrm{tr}}=\int d\,\hat{\boldsymbol{k}}'\,\hat{\boldsymbol{v}}\cdot(\hat{\boldsymbol{k}}-\hat{\boldsymbol{k}}')|f(\boldsymbol{k},\hat{\boldsymbol{k}}')|^2. \tag{33}$$

Expression (32) provides the required connection with Eq. (31). We discuss in Appendix A the behavior of the stopping power as a function of velocity for low velocities.

III. RESULTS

A. Comparison with linear theory for Z small

The numerical solution of the coupled equations can be checked when perturbation theory is valid. For a given potential $\lambda V(\boldsymbol{r})$, the transition amplitude (12) for small λ is given by the first Born expression

$$f^B(\boldsymbol{k},\hat{\boldsymbol{k}}')=8\pi\lambda\sum_{\nu}\sum_{ll'm}(-)^m i^{l-l'}Y_{lm}(\hat{\boldsymbol{k}}')Y^*_{l'm}(\hat{\boldsymbol{k}})\times(2\nu+1)^{-1}\begin{Bmatrix} l & l' & \nu \\ m & -m & 0\end{Bmatrix}I_{ll'\nu}, \tag{34}$$

where

$$I_{ll'\nu}=\int_0^\infty r^2\,dr\,j_l(kr)j_{l'}(kr)V_\nu(r)$$

and j_l is the regular spherical Bessel function of order l. We have compared the transition amplitude obtained from the solution of the coupled equations with the Born value (34) and find very good agreement for small values of λ.

The whole procedure may be further checked by comparing our results with those of linear theory. If the exchange-correlation contribution is neglected, then our calculations should be entirely equivalent, for a small projectile charge, to results based on the RPA response function[20] (hereafter, we refer to such calculations as linear theory). We give in Fig. 1 the potential for a projectile charge of -0.01 moving with a velocity of 0.4 a.u. through a gas of $r_s=2.07$. Very good agreement is obtained for all components of the potential. Similar agreement has been obtained for the components of the density.

Alternatively, one may use our theory to gauge the role of the exchange-correlation contribution in linear theory. This is done in Fig. 2 where we give our results with and without exchange correlation for the same conditions as in Fig. 1. We see that the difference is not negligible, which proves the limitation of the RPA approximation to the response function.[21] In particular, the stopping power is significantly different in both calculations. Let us define the quantity

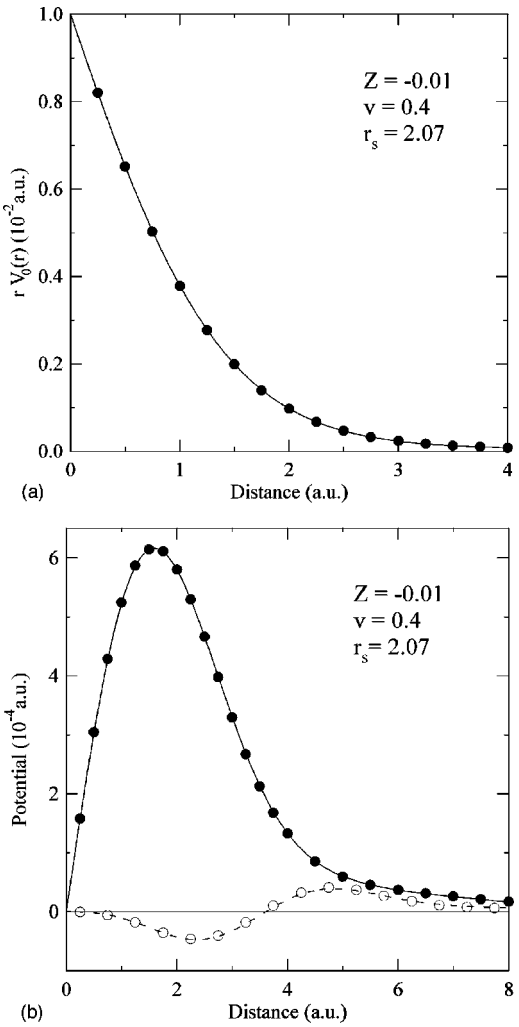

FIG. 1. Comparison of the potential (calculated without exchange-correlation) for a projectile charge -0.01 and a velocity of 0.4 a.u. (lines) with linear theory (circles): (a) monopolar component of the potential multiplied by r, (b) dipolar (full line and circles) and quadrupolar (dashed line and open circles) components of potential.

$$\mathcal{S}=\lim_{v\to 0}\frac{1}{vZ^2}\frac{dE}{dR}. \tag{35}$$

For $r_s=2.07$ and $Z=-0.01$, we get $\mathcal{S}=0.159$ a.u. without and 0.22 a.u. with exchange correlation.

B. Density

1. Comparison with spherical average

Our calculations may be checked against those of the spherical average approximation,[11] which corresponds to $\nu_{\max}=0$. Good agreement is obtained for the antiproton case considered in Ref. 11. We have plotted in Fig. 3 the density

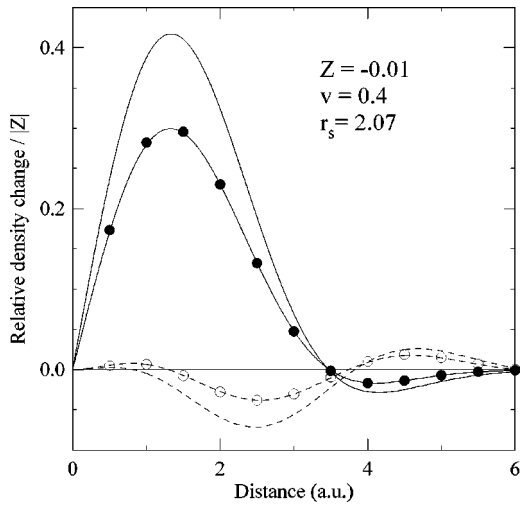

FIG. 2. Relative density change for a projectile charge -0.01 and a velocity of 0.4 a.u. calculated with (lines) and without (lines with circles) exchange correlation: dipolar (full lines) and quadrupolar (dashed lines) component of density. Circles correspond to the results of linear theory.

along the direction of the projectile velocity for $r_s=2.07$ for the nonspherical case. One can see a forward-backward asymmetry that increases with increasing projectile velocity, in good agreement with the calculations of Ref. 11. We have plotted in Fig. 4 the density obtained in the spherical and nonspherical calculations for a velocity of 0.8 a.u. There is a significant difference for the antiproton case. The asymmetry of the density is significantly reduced in the present calculations, particularly in the backward direction. The structure in the forward direction has completely disappeared. In our calculations, the asymmetry of the density is due to both the asymmetry in the potential and the integration over a shifted Fermi sphere. Only the latter source of asymmetry is present in the spherical approximation. This means that, when a fully self-consistent calculation of the potential and charge density is performed at finite velocities, the asymmetry of the potential compensates partially the asymmetry caused by the shift of the Fermi sphere in the evaluation of the density. We may observe this effect directly by looking at the various components of the potential (Fig. 1). In fact, the dipolar component of the induced potential has a sign opposite to that of the monopolar one close to their respective maxima. This is easy to understand. Because of the shift in the Fermi sphere, in the case of antiprotons, the density change is smaller in the forward than in the backward direction. In the forward direction the total density is larger and produces more screening. Therefore the induced potential is weaker, which decreases the asymmetry in the density with respect to the spherically symmetric approximation. This variation of the density is of utmost importance if one calculates the stopping power from Eq. (31). If one fails to account for the asymmetry in the density caused by the asymmetry in the potential used to determine the Kohn-Sham orbitals, then the latter procedure gives an incorrect value, even for vanishingly small velocities. This is explained in Appendix A. In contrast, the difference is much smaller between the present calculations and those of the spherical approximation for the case of protons.

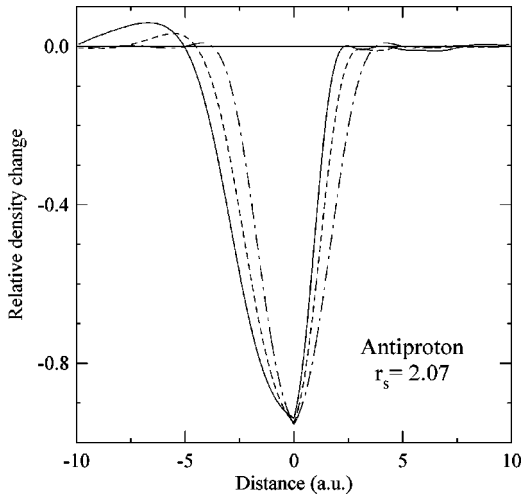

FIG. 3. Relative density change along the projectile velocity for an antiproton traveling through a jellium with density $r_s=2.07$ with velocity 0 (dash-dotted line), $v_F/2$ (dashed line) and 0.8 a.u. (full line).

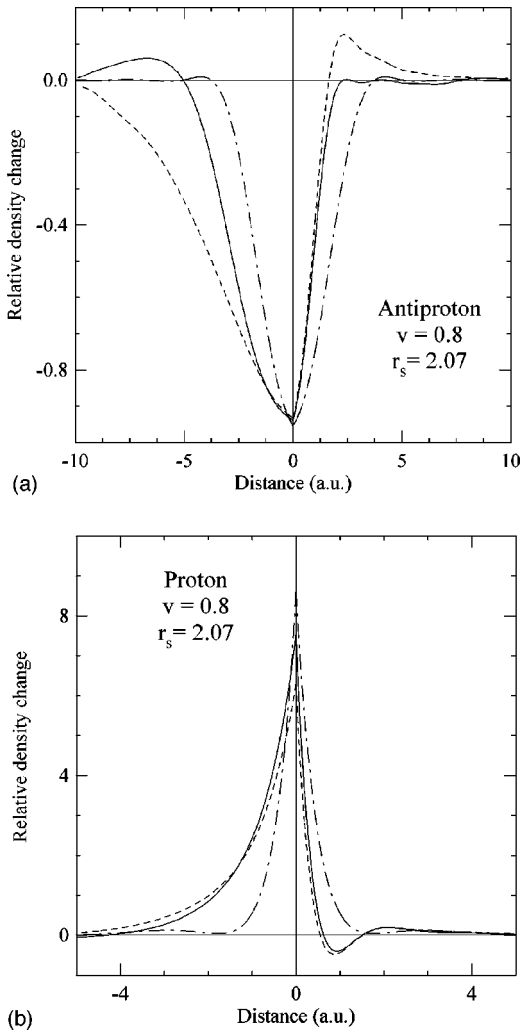

FIG. 4. Relative density change along the projectile velocity for $v=0.8$ a.u. and $r_s=2.07$. The projectile is an antiproton (a) or a proton (b). Our results (full line) are compared with those of the spherical approximation (Ref. 11) (dashed line) and of the static case (dash-dotted line).

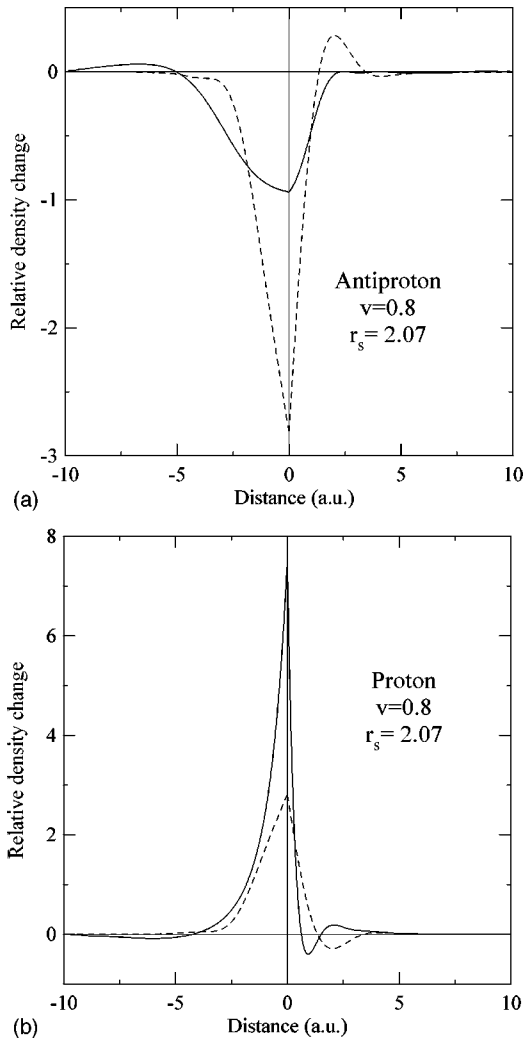

FIG. 5. Relative density change along the projectile velocity for an antiproton (a) and a proton (b) with velocity 0.8 a.u. and $r_s = 2.07$. Our results (full line) are compared with linear theory (dashed line).

The density variation is much more localized in the case of protons [note the scale difference in the x axis of Figs. 4(a) and 4(b)]: the maximum at the position of the proton is 7.5 whereas it is only -0.94 for the antiproton case.

2. Comparison with linear theory

The difference with linear theory has been already illustrated in the spherical approximation for antiprotons.[11] A similar comparison is given in Fig. 5. At the antiproton position, linear theory gives a relative depletion of $\simeq -3$. Such an unphysical value is a frequent feature of perturbation theory when it breaks down. Furthermore, this overestimation of the depletion at the antiproton position produces a reduction of the range of the density variation and of the asymmetry. For a proton, linear theory underestimates the density at the proton by a factor of roughly 2.5. It therefore overestimates the asymmetry, which is reduced in our calculations by the large screening of the nuclear charge.

3. Friedel oscillations

The usual Friedel oscillations in the density are seen far from the projectile at low velocities. We plot in Fig. 6 the

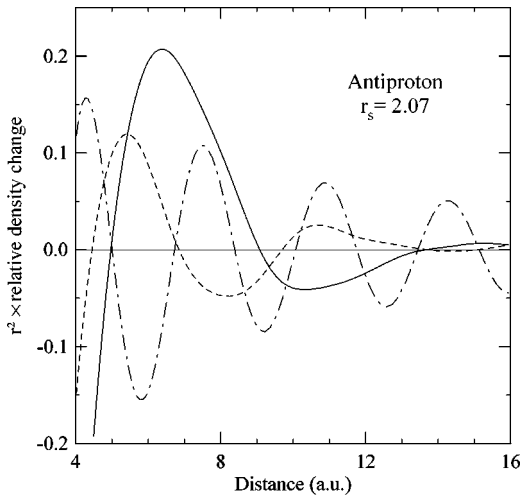

FIG. 6. Friedel oscillations for various velocities. The relative monopolar density change multiplied by r^2 is shown for an antiproton with velocity 0 (dash-dotted curve), $v_F/2$ (dashed curve) and 0.8 a.u. (full curve) in a jellium with density $r_s = 2.07$.

monopolar part of the density for the static case and for finite velocities. The other multipolar components of the density show similar oscillations. It can be clearly seen that the frequency of the oscillations and their amplitude decrease when the velocity increases. A similar effect has been found in Ref. 22 for a hard sphere moving in a jellium. This effect can be related to the shift in the Fermi distribution. As shown in Eq. (B12), the density arises from an integration over k weighted by the function $\mathcal{C}^m(k)$. For the static case, $\mathcal{C}^m$ is independent of k and the integration over k yields a single oscillating term having a frequency π/k_F. For finite velocities and $v < k_F$, $\mathcal{C}^m$ is also constant for $v < k_F - v$ so the integral over k from 0 to $k_F - v$ gives a single oscillating term with frequency $\pi/(k_F - v)$ and a smaller amplitude. The contribution for $k > k_F - v$ is smaller because $\mathcal{C}^m(k)$ decreases rapidly with k and it is partially quenched by interferences. This explains qualitatively the observed behavior. Physically, it comes from the fact that the density oscillations far from the projectile are an average over density waves having a distribution of wave vectors the center of gravity of which is v (instead of zero for the static case). The interference pattern is characterized by a beating frequency of the order of $\pi/(k_F - v)$ and a smaller amplitude.

C. Stopping power

We give in Fig. 7 the energy loss for various values of Z. In all cases, the occupation of the bound states has been set to zero. We have also included, for the sake of comparison, the unphysical case $Z = 0.5$. The most striking result is the linearity of the energy loss as a function of velocity for all cases up to velocities close to the Fermi energy. The largest deviation with respect to linearity is observed for protons. As is well known, it can be proved that the energy loss tends to zero linearly with velocity when the velocity v tends to zero ($v \ll v_F$). However, until now, no evaluation was available on the importance of higher orders in v for the Taylor expansion of the stopping power at low velocities. Our calculations show that linearity is observed up to velocities close to the Fermi velocity. The same conclusion was reached with

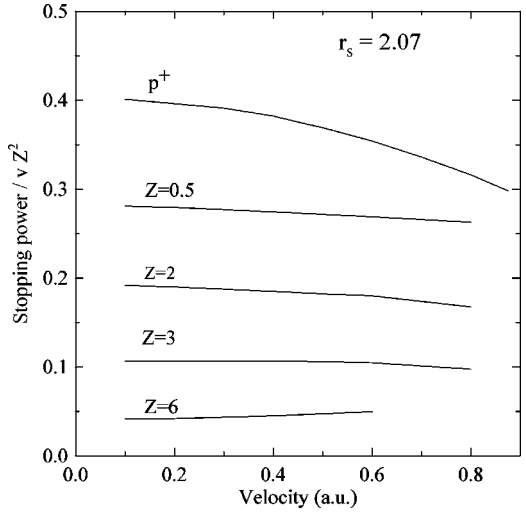

FIG. 7. Stopping power (in a.u.) divided by vZ^2 as a function of velocity for various projectiles and $r_s=2.07$.

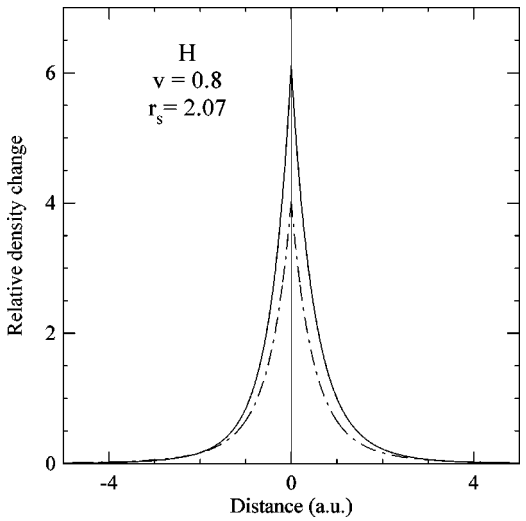

FIG. 8. Contribution of the H bound state to the relative density change along the projectile velocity for $v=0.8$ and $r_s=2.07$ (full curve) compared to that of the static case (dash-dotted curve).

the nonlinear hydrodynamic theory[7] (note that the calculations for protons in the latter work should be compared to our results for H discussed in Sec. III D). The consequence of this linearity with velocity is that the variation with Z is very close to the one already observed for the static case.[23] In addition to being farther from linearity, the proton stopping corrresponds to a maximum in the dependence over Z of the stopping power divided by Z^2.

D. Bound states

We have carried out a spin-polarized calculation for the case of *H*, which means that we have accounted for a singly occupied bound state. We give in Table I the Kohn-Sham eigenenergies as a function of velocity for two different values of r_s. We are well aware of the fact that the Kohn-Sham eigenvalues should be considered with some caution and that they cannot be interpreted as an ionization energy. However, we are more interested here in trends than in absolute values. The evolution of the Kohn-Sham eigenvalues as a function of velocity is representative of the effect of dynamic screening on the bound states. As expected, we see that the binding energy increases with increasing velocity, i.e., the bound state becomes less sensitive to the presence of the jellium as the velocity increases. This behavior is at variance with the one found in Ref. 24: the latter authors found that the bound-state energy increases with velocity for low velocities.

The density of the bound state shown in Fig. 8 is larger in the forward direction than in the backward direction, which means that the bound electron feels an attraction toward the forward direction (less screening by continuum electrons). This is more clearly seen in Fig. 9 where we plot the asymmetry in the density as a function of $|z|$. This asymmetry is defined as $2[n^B(+)-n^B(-)]/[n^B(+)+n^B(-)]$. The asymmetry of the continuum density has two different origins. One is the shift in the Fermi distribution, the other in the asymmetry of the potential. It is the asymmetry in the shifted Fermi distribution that produces a smaller electronic density in the forward direction for a positive ion. We have shown already that the asymmetry of the potential creates a density change in the opposite direction, precisely because of the lower density in the forward direction caused by the shifted Fermi distribution. The same effect can be seen in the total density in the present case. However, the bound-state density is not determined by integration over a Fermi distribution. Therefore the asymmetry of the bound-state density arises only from the asymmetry of the potential. This is the

TABLE I. Orbital energies of H (in a.u.).

v (a.u.)	$r_s=2.07$	$r_s=3$
0.0	−0.0203	−0.0892
0.1		−0.0902
0.2	−0.0231	−0.0928
0.3		−0.0968
0.4	−0.0300	−0.1022
0.5	−0.0343	−0.1090
0.6	−0.0394	
0.8	−0.0500	

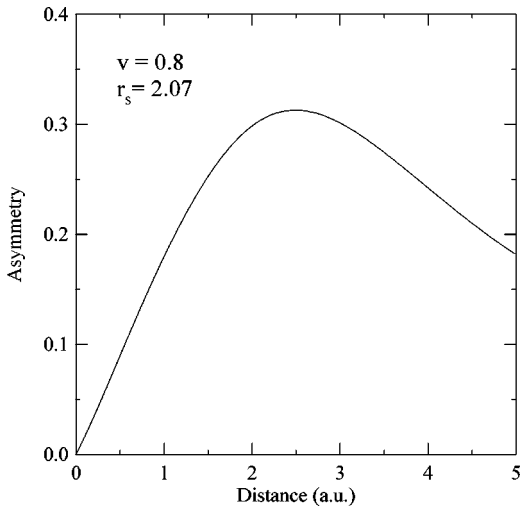

FIG. 9. Relative asymmetry of the density for a H atom with velocity 0.8 a.u. traveling through a jellium with $r_s=2.07$.

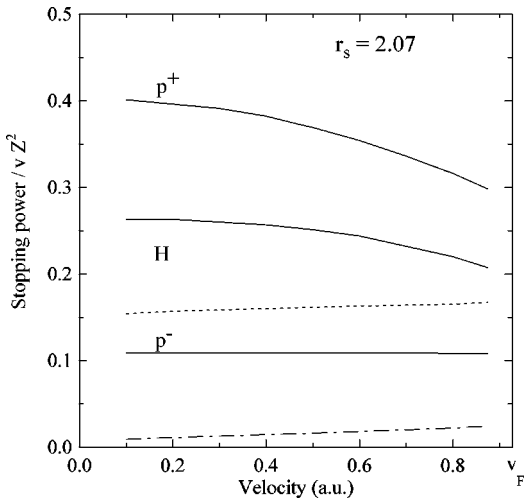

FIG. 10. Stopping-power (in a.u.) divided by vZ^2 as a function of velocity for various projectiles and $r_s = 2.07$. The dashed curve gives the result of linear theory and the dash-dotted curve the energy gain by the bound electron for the case of H.

reason why the bound state has an asymmetry opposite to that of the continuum and total densities. This effect can only be seen in a self consistent calculation, i.e., when the potential fully accounts for the asymmetry caused by the projectile motion.

As shown in Fig. 10, the H stopping is smaller than the proton stopping. This reduction is caused by the smaller asymmetry in the screening of the proton field for the H case though the density itself is larger at the origin for H than for protons (see Table II). Part of this reduction may be related to the previous discussion on the asymmetry of the bound state. Expression (31) shows the direct relation between the density asymmetry and the stopping power. Therefore the bound state density gives a contribution to the stopping power opposite that of the continuum. In fact, the forward-backward asymmetry in the density of continuum electrons produces an attraction of the bound electron in the forward direction. This means that the interaction of the bound electron with the continuum electrons produces an energy gain (as the electronic state is stationary in the projectile frame, we may consider that the bound electron-proton system evolves as a rigid body). In other terms, the reduction of the energy loss for a H atom compared to the proton one has two different origins. One is due to the change in screening by the unbound electrons caused by the presence of a bound state. The other is due to the attraction of the bound electron in the forward direction (this effect arises to first order in v from the dipolar term of the potential). The contribution associated with the energy gain by the bound electron is much smaller than the one due to screening (see Fig. 10). It is interesting to note that the evaluation of the stopping power in the projectile frame through the transport cross section (32) includes automatically these two effects through the Kohn-Sham potential. In fact, the Kohn-Sham potential accounts for the interaction of any electron with all electrons, whether they are bound or not.

TABLE II. Relative density change at the origin.

v (a.u.)	Antiproton	Proton	H
0.0	−0.954	8.60	17.5
0.2	−0.953	8.52	17.3
0.4	−0.951	8.35	16.8
0.5	−0.950	8.25	16.5
0.6	−0.947	8.10	16.0
0.8	−0.939	7.52	14.9

IV. CONCLUSION

We have shown that an ensemble Kohn-Sham calculation of the dynamical screening of an ion moving in an electron gas is feasible. It allows therefore to determine self-consistently the perturbation of the medium by the moving projectile. The virtue of the method is that it allows an unambiguous definition of the bound electronic orbitals moving with the projectile. The perturbed continuum orbitals represent the projectile wake, i.e., a perturbation of the medium moving with the projectile. Bound and continuum orbitals are orthogonal at any time since they are solutions of the same Kohn-Sham equations. We have shown that the asymmetry of the potential creates an asymmetry in the bound states that is the opposite of the one produced on the total density by the projectile motion: the bound electron feels a net attraction in the forward direction. It would be of great interest to study the relevance of these features to electron capture and loss processes.[25]

We have completed the proof of the linearity in the variation of the stopping power with velocity at low velocities. We have extended the derivation of the Friedel sum rule and oscillations by fully taking into account the cylindrical symmetry of the potential at finite velocities. We have found that the stopping power of the electron gas is nearly linear (in velocity) up to the Fermi velocity, the largest deviation being observed for the case of protons (moving with no bound electron). This is in accord with previous findings with the spherical average[11] and nonlinear hydrodynamic[7] approximations.

The main limitation of the present method of solution lies in the use of spherical coordinates and in convergence difficulties with the iterative solution of the Kohn-Sham equations when the velocity increases. This has limited its use, in the present work, to velocities below the Fermi velocity.

ACKNOWLEDGMENTS

We wish to thank I. Nagy and V.H. Ponce for useful discussions. A.S. wishes to thank his colleagues of the Materialeen Fizika Saila at the Euskal Herriko Unibertsitatea for their kind hospitality while this work was performed and the Iberdrola Foundation for support. This work has been partially supported by the DGICYT of the Ministerio de Educación y Ciencia and the Fonds Commun de Coopération Aquitaine-Euskadi (Conseil Régional d'Aquitaine-Euskal Jaurlaritza).

APPENDIX A: STOPPING POWER AT LOW VELOCITIES

The usual proof that the stopping power varies linearly with velocity for low velocities is based on its relation with the transport cross section calculated *with a spherically sym-*

metric potential.[19] The linearity in v then arises from the shift in the Fermi sphere. However, for nonzero velocities, the potential has multipolar components and the dipolar component is linear in v for small v. The previous proof is therefore incomplete as long as the contribution of the dipolar component of the potential has not been evaluated.

We treat the problem first in the projectile frame. The energy given by an electron with momentum $\boldsymbol{k}$ scattered by a projectile of infinite mass and velocity $\boldsymbol{v}$ into the direction $\boldsymbol{k}'$ is $\boldsymbol{v}\cdot(\boldsymbol{k}-\boldsymbol{k}')$. The average over all possible scattering directions and all electrons gives

$$\frac{dE}{dR}=\frac{1}{4\pi^3}\int^{\mathrm{SFS}} d\boldsymbol{k}\int d\hat{\boldsymbol{k}}'\; k\hat{\boldsymbol{v}}\cdot(\boldsymbol{k}-\boldsymbol{k}')|f(\boldsymbol{k},\hat{\boldsymbol{k}}')|^2, \quad \text{(A1)}$$

where the sum over $\boldsymbol{k}$ is over a shifted Fermi sphere as explained earlier. The contribution, to first order in v, of the monopolar term of the potential, V_0, has already been derived.[19] The dipolar component of the potential V_1 is linear in v. Therefore, to first order in v, the contribution of the dipolar component of the potential to the energy loss may be calculated from the energy loss dE_1/dR caused by the dipolar potential alone when the integration over $\boldsymbol{k}$ is over an unshifted Fermi sphere:

$$\frac{dE_1}{dR}=\frac{1}{4\pi^3}\int_0^{k_F}k^2\,dk\int d\hat{\boldsymbol{k}}\int d\hat{\boldsymbol{k}}'\; k\hat{\boldsymbol{v}}\cdot\boldsymbol{k} \times(|f_1(\boldsymbol{k},\hat{\boldsymbol{k}}')|^2-|f_1(\boldsymbol{k}',\hat{\boldsymbol{k}})|^2). \quad \text{(A2)}$$

This contribution is not zero in general, because of the asymmetry of the potential, as can be checked from the form of the transition amplitude (12). However for vanishingly low velocities, one may use the Born approximation (34) which verifies the condition $f(\boldsymbol{k},\hat{\boldsymbol{k}}')=f^*(\boldsymbol{k}',\hat{\boldsymbol{k}})$ and, therefore, the quantity dE_1/dR is of order v^2 at least. So the previous derivation of the low-velocity limit of the stopping power yields the correct result in spite of its incompleteness: the transport cross section may be calculated, in this limit, from V_0 only.

Let us calculate now the energy loss in the electron gas frame. We call $\hat{H}(t)$ the Hamiltonian describing the electron motion in the field of the moving ion. Let $\Psi_i(t)$ be the solution of the time-dependent Schrödinger equation. The energy lost by the projectile per unit path length is

$$\frac{dE}{dR}=-\frac{1}{v}\frac{d}{dt}\langle\Psi_i(t)|\hat{H}(t)|\Psi_i(t)\rangle \quad \text{(A3)}$$

$$=-\frac{1}{v}\langle\Psi_i(t)|\frac{d\hat{H}(t)}{dt}|\Psi_i(t)\rangle. \quad \text{(A4)}$$

The last step follows from the time-dependent Schrödinger equation. Using the fact that the time dependence of $\hat{H}(t)$ arises entirely from the projectile potential and that the latter is a one-electron operator, the previous expression may be cast into the form

$$\frac{dE}{dR}=\frac{Z}{v}\int d\boldsymbol{r}\; n[\boldsymbol{r}-\boldsymbol{R}(t)]\frac{d}{dt}\left(\frac{1}{|\boldsymbol{r}-\boldsymbol{R}(t)|}\right). \quad \text{(A5)}$$

The dependence of n on time is fixed by our adiabatic approximation, which gives a constant density in the projectile frame. We therefore obtain the result (31), which proves the equivalence between Eq. (31) and the expression in terms of the transport cross section (32). Using Poisson's equation one shows immediately that

$$\frac{dE}{dR}=Z\int d\boldsymbol{r}\; n_1(\boldsymbol{r}). \quad \text{(A6)}$$

However, for the result (A6) to give correctly the linear dependence at low velocities, it is essential that the density $n_1(\boldsymbol{r})$ be calculated with both the monopolar *and* dipolar components of the potential. In fact, the above proof of Eq. (A6) assumes that $\Psi_i(t)$ is solution of the time dependent Schrödinger equation. We only get correctly the term linear in v if $\Psi_i(t)$ is correct to first order in v. The dipolar component of the potential indeed gives a contribution to the density that is linear in v. We have checked in actual calculations that the results are grossly in error if the density is calculated from V_0 only. Our self-consistent calculations obviously satisfy this criterium and both expressions for the energy loss give the same results.

APPENDIX B: FRIEDEL SUM RULE AND FRIEDEL OSCILLATIONS FOR FINITE VELOCITIES

The well-known Friedel sum rule and Friedel oscillations can be readily obtained for finite velocities from our previous expressions. The total variation of the screening density can be written as

$$Z=N_B+N_C=N_B+\int d\boldsymbol{r}\;\Delta n^C(\boldsymbol{r})=N_B+\int d\boldsymbol{k}\,\Delta n^C_{\boldsymbol{k}}, \quad \text{(B1)}$$

where $\Delta n^C(\boldsymbol{r})$ gives the variation in density due to the continuum states and N_B is the total number of electrons in bound states.[26] By definition and for a spin-unpolarized calculation (the generalization to spin-polarized calculations is trivial),

$$N_C=2\int d\boldsymbol{k}\int d\boldsymbol{r}\{|\psi_{\boldsymbol{k}}|^2-|\phi_{\boldsymbol{k}}|^2\}. \quad \text{(B2)}$$

From the Schrödinger equation

$$\begin{aligned}(k^2-k'^2)\int d\boldsymbol{r}\{\psi_{\boldsymbol{k}}\psi^*_{\boldsymbol{k}'}+\psi^*_{\boldsymbol{k}}\psi_{\boldsymbol{k}'}\}&\\ =-\int d\boldsymbol{r}\{[\psi^*_{\boldsymbol{k}'}\nabla^2\psi_{\boldsymbol{k}}-\psi_{\boldsymbol{k}}\nabla^2\psi^*_{\boldsymbol{k}'}]+\text{c.c.}\}&\\ =-\lim_{r\to\infty}\left\{\int r^2 d\Omega_{\hat{\boldsymbol{r}}}\left[\psi^*_{\boldsymbol{k}'}\frac{d}{dr}\psi_{\boldsymbol{k}}-\psi_{\boldsymbol{k}}\frac{d}{dr}\psi^*_{\boldsymbol{k}'}\right]+\text{c.c.}\right\}.&\end{aligned} \quad \text{(B3)}$$

Introduce $k'=k+dk$ we end with

$$\int d\boldsymbol{r}|\psi_{\boldsymbol{k}}|^2=\frac{1}{2k}\lim_{r\to\infty}\left\{\int r^2 d\,\Omega_{\hat{\boldsymbol{r}}}\left[\frac{d}{dk}\psi_{\boldsymbol{k}}^*\frac{d}{dr}\psi_{\boldsymbol{k}}-\psi_{\boldsymbol{k}}\frac{d}{dk}\frac{d}{dr}\psi_{\boldsymbol{k}}^*\right]+\text{c.c.}\right\}. \tag{B4}$$

To calculate Eq. (B2), we may use the asymptotic form (7) of $\psi_{\boldsymbol{k}}$. After some elementary steps and making use of the optical theorem

$$4\pi\,\mathrm{Im}[f(\boldsymbol{k},\hat{\boldsymbol{k}})]=k\int d\Omega_{\hat{\boldsymbol{k}}'}|f(\boldsymbol{k},\hat{\boldsymbol{k}}')|^2, \tag{B5}$$

we get

$$\Delta n_{\boldsymbol{k}}^C=\left[\frac{4\pi}{k}\frac{d}{dk}f^*(\boldsymbol{k},\hat{\boldsymbol{k}})+2i\int d\Omega_{\hat{\boldsymbol{r}}}f(\boldsymbol{k},\hat{\boldsymbol{r}})\frac{d}{dk}f^*(\boldsymbol{k},\hat{\boldsymbol{r}})+\frac{4\pi}{k^2}f(\boldsymbol{k},\hat{\boldsymbol{k}})\right]\Big/(2\pi)^3. \tag{B6}$$

We have already given the expression of the transition amplitude as expression (12). By substitution and a further use of the optical theorem we obtain the final expression

$$N_C=\frac{i}{\pi}\sum_{ll'm}\int k^{-2}\,d\boldsymbol{k}\;i^{l-l'}Y_{lm}(\hat{\boldsymbol{k}})Y_{l'm}^*(\hat{\boldsymbol{k}})\left[\left(\frac{d}{dk}\boldsymbol{S}^m\right)^\dagger\boldsymbol{S}^m\right]_{l'l}. \tag{B7}$$

Performing the angular integration,

$$N_C=\frac{i}{2\pi}\sum_{ll'm}\int dk\;\mathcal{C}_{ll'}^m(k)i^{l-l'}\left[\left(\frac{d}{dk}\boldsymbol{S}^m\right)^\dagger\boldsymbol{S}^m\right]_{l'l} \tag{B8a}$$

$$=\frac{i}{2\pi}\sum_m\int dk\,\mathrm{Tr}\left[\boldsymbol{c}^m\left(\frac{d}{dk}\boldsymbol{S}^m\right)^\dagger\boldsymbol{S}^m\right], \tag{B8b}$$

where the operator $\boldsymbol{c}^m$ has matrix elements $\mathcal{C}_{ll'}^m(k)i^{l-l'}$ and Tr stands for the trace of the matrix product. For the calculation of the latter, we may use $\boldsymbol{S}^m(k)=\exp[2i\boldsymbol{D}^m(k)]$. The unitarity of the $\boldsymbol{S}^m$ operator implies that $\boldsymbol{D}^m$ is hermitic. We have $d\boldsymbol{S}^m/dk\neq 2i\boldsymbol{S}^m d\boldsymbol{D}^m/dk$ because the operators $d\boldsymbol{D}^m/dk$ and $\boldsymbol{D}^m$ usually do not commute. However, the trace of a product of operators is invariant under a change in their order which means that any commutator can be set to zero in the calculation of the trace. We end with

$$N_C=\frac{1}{\pi}\sum_m\int dk\,\mathrm{Tr}\left[\boldsymbol{c}^m(k)\frac{d\boldsymbol{D}^m}{dk}\right]. \tag{B9}$$

This expression cannot be further simplified in the general case because of the shift in the Fermi sphere, which introduces a dependence on k for the bounds on the integration over $\hat{\boldsymbol{k}}$ and therefore a dependence of the matrix $\boldsymbol{c}^m$ on k.

To make the connection with the usual sum rule, it is of interest to consider the case of a potential with cylindrical symmetry for zero velocity. Then the integration over $d\Omega_{\hat{\boldsymbol{k}}}$ is trivial and one gets $c_{ll'}^m(k)=2\,\delta_{ll'}$. If we call δ_l^m the (real) eigenvalues of $\boldsymbol{D}^m$, one obtains

$$N_C=\frac{2}{\pi}\sum_{lm}\left[\delta_l^m(k_F)-\delta_l^m(0)\right]. \tag{B10}$$

It reduces trivially to the usual expression for the case of a spherically symmetric potential since in the latter case δ_l^m does not depend on m.

The derivation of the Friedel oscillations follows similar steps. Now we calculate the limit for $r\to\infty$ in Eq. (B4) up to next order in $1/r$.

$$\Delta n^C(r)\sim_{r\to\infty}-\frac{(2\pi)^{-3}}{r^2}\frac{d}{dr}\int k^{-2}\,d\boldsymbol{k}\;\mathrm{Real}\{f(\boldsymbol{k},-\hat{\boldsymbol{k}})e^{2ikr}\} \tag{B11}$$

$$\sim_{r\to\infty}-\frac{1}{4\pi^2r^2}\times\sum_{lm}\int dk\;\mathrm{Real}\{e^{2ikr-il\pi}\,\mathrm{Tr}[\boldsymbol{c}^m\boldsymbol{S}^m-\boldsymbol{C}^m]\}. \tag{B12}$$

The integration over k to first order in $1/r$ cannot be carried out as usual because the matrix $\boldsymbol{C}^m$ is zero at the maximum value of k. Furthermore, $\boldsymbol{C}^m$ decreases rapidly for $k>k_F-v$ (when $v<k_F$), which explains why the frequency of the Friedel oscillations decreases when the velocity increases. The dependence of $\boldsymbol{C}^m$ on k also explains the decrease in the amplitude of these oscillations.

[1] E. Fermi and E. Teller, Phys. Rev. **72**, 399 (1947).

[2] D. Bohm and D. Pines, Phys. Rev. **82**, 625 (1951); **92**, 609 (1953).

[3] J. Lindhard, K. Dan. Vidensk. Selsk. Mat. Fys. Medd. **28**, 8 (1954).

[4] J. Neufeld and R. H. Ritchie, Phys. Rev. **98**, 1632 (1955).

[5] J. S. Lander and S. H. Vosko, J. Phys. Chem. Solids **12**, 196 (1960); H. Stachowiak, Bull. Acad. Pol. Sci., Ser. Sci., Math., Astron. Phys. **23**, 1213 (1975); A. Mazarro, P. M. Echenique, and R. H. Ritchie, Phys. Rev. B **27**, 4117 (1983).

[6] C. C. Sung and R. H. Ritchie, Phys. Rev. A **28**, 674 (1983); C. D. Hu and E. Zaremba, Phys. Rev. B **37**, 9268 (1988); H. Esbensen and P. Sigmund, Ann. Phys. (N.Y.) **201**, 152 (1990); J. M. Pitarke, R. H. Ritchie, and P. M. Echenique, Nucl. Instrum. Methods Phys. Res. B **79**, 209 (1993); Phys. Rev. B **52**, 13 883 (1995).

[7] E. Zaremba and A. Arnau, Nucl. Instrum. Methods Phys. Res. B **90**, 32 (1994).

[8] J. J. Dorado, O. H. Crawford, and F. Flores, Nucl. Instrum. Methods Phys. Res. B **93**, 175 (1994); **95**, 144 (1995).

[9] C. O. Almblahd, U. von Barth, Z. D. Popović, and M. J. Stott, Phys. Rev. B **14**, 2250 (1976); E. Zaremba, L. M. Sander, H. B. Shore, and J. H. Rose, J. Phys. F **7**, 1763 (1977).

[10] P. M. Echenique, R. M. Nieminen, J. C. Ashley, and R. H.

Ritchie, Phys. Rev. A **33**, 897 (1986).
[11] E. Zaremba, A. Arnau, and P. M. Echenique, Nucl. Instrum. Methods Phys. Res. B **96**, 619 (1995).
[12] K. Schönhammer, Phys. Rev. B **37**, 7735 (1988).
[13] R. M. Dreizler and E. K. U. Gross, *Density Functional Theory* (Springer-Verlag, Berlin, 1990).
[14] W. H. Press, S. A. Teukolsky, W. T. Vetterling, and B. P. Flannery, *Numerical Recipes* (Cambridge University Press, Cambridge, 1992).
[15] A. Arnau, P. A. Zeiljmans van Emmichoven, J. L. Juaristi, and E. Zaremba, Nucl. Instrum. Methods Phys. Res. B **100**, 279 (1995).
[16] P. M. Echenique, I. Nagy, and A. Arnau, Int. J. Quantum Chem., Quantum Chem. Symp. **23**, 521 (1989).
[17] M. Abramowitz and I. A. Stegun, *Handbook of Mathematical Functions* (Dover, New York, 1965).
[18] O. Gunnardson and B. I. Lundqvist, Phys. Rev. B **13**, 4274 (1976).
[19] P. M. Echenique and M. E. Uranga, *Interaction of Charged Particles with Solids and Surfaces*, edited by A. Gras-Martí *et al.* (Plenum, New York, 1991).
[20] J. Lindhard, K. Dan. Vidensk. Selsk. Mat. Fys. Medd. **34**, 14 (1965).
[21] I. Nagy, J. László, and J. Giber, Z. Phys. A **321**, 221 (1985); B. Dabrowski, Phys. Rev. B **34**, 4989 (1986); I. Nagy, A. Arnau, and P. M. Echenique, *ibid.* **38**, 9191 (1988).
[22] L. Bönig and K. Schönhammer, Phys. Rev. B **39**, 7413 (1989).
[23] P. M. Echenique, A. Arnau, M. Peñalba, and I. Nagy, Nucl. Instrum. Methods Phys. Res. B **56/57**, 345 (1991).
[24] F. Guinea, F. Flores, and P. M. Echenique, Phys. Rev. B **25**, 6109 (1982).
[25] P. M. Echenique, F. Flores, and R. H. Ritchie, Solid State Phys. **43**, 229 (1990).
[26] For spin unpolarized calculations, this is twice the number of bound states.